CHAPTER II
LITERATURE REVIEW

In 1997, Suong H. *et al.*, provided the information on the synthesis of PLA having a wide range of molecular weights. In the study PLA with different molecular weights was synthesized with the conversional polycondensation (condensation polymerization) of lactic acid and ring-opening polymerization of lactide focusing on the effects of catalyst concentration, polymerization time, and polymerization temperature on the polymer yield, molecular weight, and optical rotation. The synthesis of PLA through polycondensation of lactic acid monomer gave weight average molecular weights (M_w) lower than $1.6x10^4$, whereas ring-opening polymerization of lactide in bulk using stannous as catalyst produced PLA with viscosity average molecular weight (M_v) ranging from $2x10^4$ to $6.8x10^5$. The monomer conversion and M_v showed a maximum at a catalyst concentration around 0.05%. The monomer conversion and M_v increased almost linearly with polymerization time up to a monomer conversion of 80%, but both the conversion and M_v decreased after passing through a maximum, when the polymerization reaction was allowed to proceed for longer period of time. This time dependence was pronounced at higher polymerization temperature. The decrease in M_v at prolonged polymerization and higher polymerization temperature was attributed to thermal depolymerization of resultant polylactides, but no significant optical rotation of poly(L-lactide) was noticed.

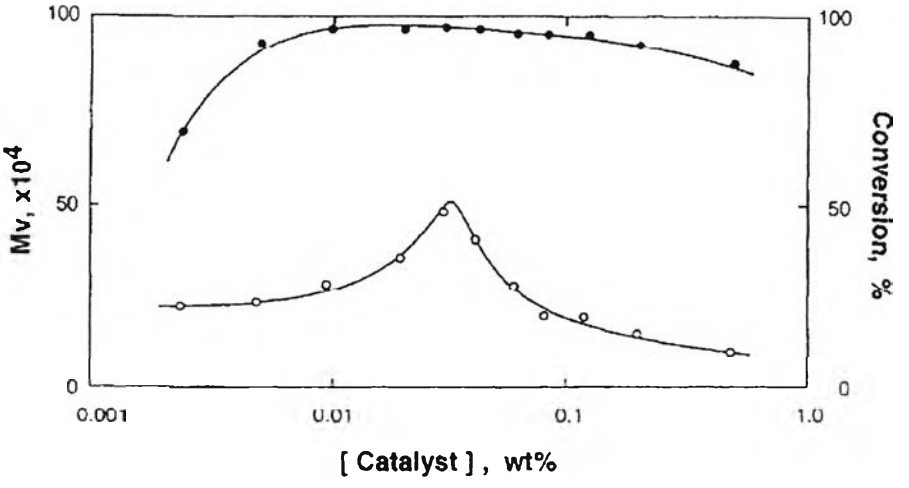

Figure 2.1 Effect of stannous octoate concentration o the viscosity average molecular weight of poly(L-lactide) and monomer conversion for bulk polymerization of L-lactide at 130 °C for 72 h. o:molecular weight, •:conversion.

Jacobsen S. *et al.*, (2000) studied the effect of triphenylphosphine on the efficiency of tin(II) 2-ethylhexanoate as a catalyst for the ring opening polymerization of L,L-lactide into polylactide. It was the starting point to use reactive extrusion technology to produce PLA. Reactive extrusion technology promoted by equimolar $Sn(Oct)_2{\cdot}P(\phi)_3$ complex was compared to batch polymerization technology on the basis of molecular parameters number average molecular weight (M_n), molecular weight distribution (MWD), and conversion rate (c). The resulting conversions, 98.5% in glass ampoule bulk batch polymerization and 99% in single stage reactive extrusion, showed that in both cases the polymerization reaction had been finished (Table 2.1). Though for the bulk batch polymerization in glass ampoule the time required to reach this conversion was approximately 40 min compared with only 7-8 min in the reactive extrusion process. The difference could be explained by the fact that as soon as a high molecular weight, i.e. a high melt viscosity is reached, the speed of reaction was limited by the diffusion of the dimers or the low molecular weight compounds inside the high viscosity melt. The low MWD-values smaller than 2 in both cases showed that intermolecular transisterification reactions had been very limited, which was due to the use of triphenylphosphine as a catalyst. The dif-

ference in molecular weight could be explained by the fact that the lactide in the glass ampoule has been recrystallised, while it had been used as received for reactive extrusion polymerization. Moreover, the processing and screw concept was developed to polymerize L,L-lactide into PLA using a closely intermeshing corotating twin-screw extruder. The effect of the main processing parameters such as screw speed (n), throughput rate (m), and extruder head pressure (p) on the molecular parameters was determined. All processing parameters and the molecular parameters of the resulting polymers were gathered comparison in Table 2.2. The conversion would decrease by increasing the mass flow rate and screw speed. The fact could be explained by the residence time of material inside the extruder. The molecular weight increased as increase in the mass flow rate and extruder head pressure. The molecular weight distribution decreased slightly, while increasing the mass flow rate and screw speed that could be explained by degradation reaction. Finally; the resulting PLA-polmers were analyzed by means of their physico-mechanical property profile. They exhibited thermal and mechanical properties which allowed polylactide to be used in a wide range of nowadays polymer application.

Table 2.1 Comparison of two types of poly-L-lactide polymerized in glass ampoule bulk batch polymerization technology and using a single stage reactive extrusion polymerization process, both catalyzed with equimolar $Sn(Oct)_2 \cdot P(\phi)_3$ complex with an initial monomer to tin molar ratio of 5000 at 180 °C

Entry	Process	$M_n x 10^{-3}$	M_w/M_n	Conversion (%)	Time (min) for conversion
1	Grass ampoule	246.0	1.9	98.5	40
2	REX	91.1	1.8	99.0	~7

Table 2.2 Influence of different processing parameters during reactive extrusion polymerization on the resulting molecular polymer parameters

Entry	Screw speed (rpm)	Mass flow rate (kg/h)	Extruder head pressure (bar)	$M_L \times 10^{-3}$ [a]	M_w/M_n [a]	Conversion (%) [b]	Origin of PLA
1	50	0.75	~30	77.0	1.80	99	2B
2	50	1.00	~30	81.0	1.70	97	2B
3	50	1.25	~30	66.0	2.10	94	2B
4	50	1.00	~35	83.0	1.70	94	Boehringer
5	100	1.00	~35	79.0	1.70	90	Boehringer
6	200	1.00	~35	81.0	1.80	87	Boehringer
7	100	1.00	~40	79.0	1.70	94	2B
8	100	1.00	~60	84.0	1.70	94	2B
9	100	1.00	~85	86.0	1.80	96	2B
10	100	1.00	~110	89.5	1.75	(92)	2B

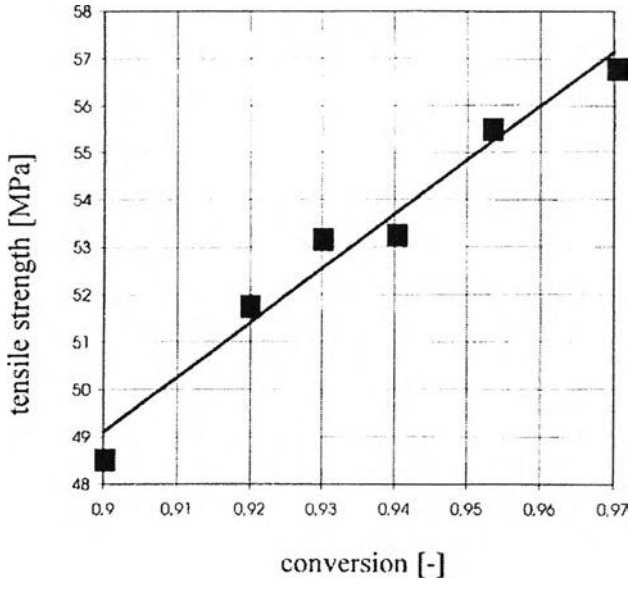

Figure 2.2 Tensile strength as a function of reached degree of conversion for poly-l-lactide produced in reactive extrusion polymerization.

At the same time, Jacobsen S. *et al.*, (2000) produced polylactide (PLA) continuously in larger quantities and at lower costs than before based on a new catalytic system and a reactive extrusion polymerization process. There were cyclic monomers or comonomers which used for ring opening polymerization by using reactive extrusion technology (Fig. 2.3). This extrusion polymerization process had been developed and tested with laboratory scale machines and the possibilities to extend this polymerization process to lactide based blockcopolymers had been investigated. One could generate a blockcopolymer of defined composition and with defined blocklength of the second monomer by using large amount of prepolymers and $Sn(Oct)_2$ as catalyst. The production of blockcopolymers made of hydroxyterminated pre-oligomerised block of one monomer and lactide as second monomer had been presented in Fig. 2.4. By adopting the length of the pre-oligomerised blocks as well as the total amount of blocks added, a multitude of possible blockcopolymers could be generated with the same processing concept and equipment to receive polymers with different mechanical, physical, thermal, and biodegradable properties for different applications.

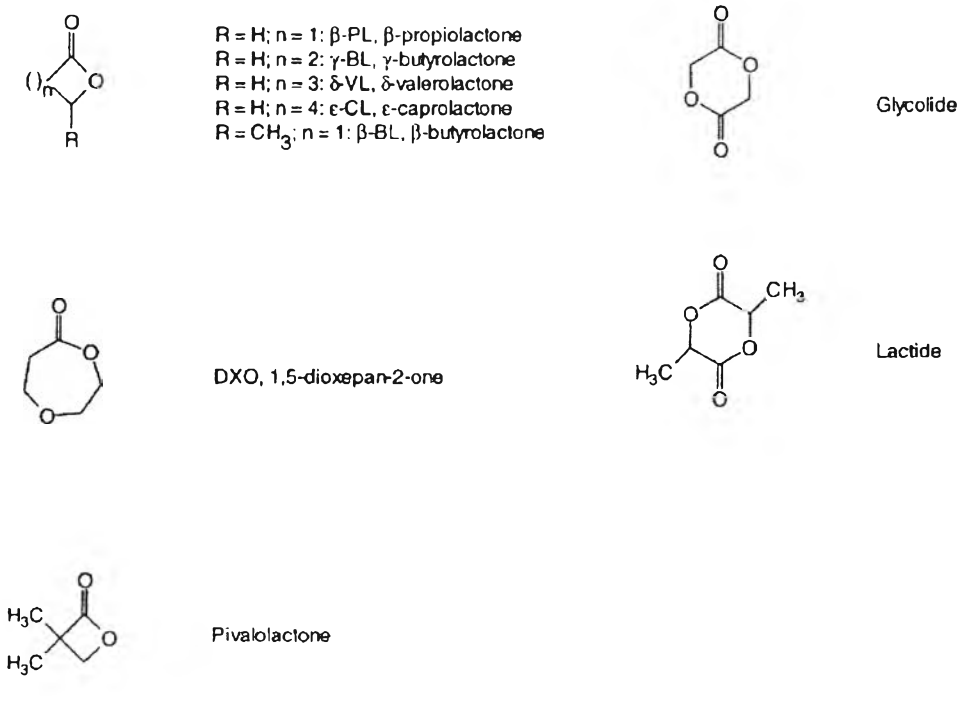

Figure 2.3 Cyclic monomers or dimers to be used for ring opening polymerization using reactive extrusion technology.

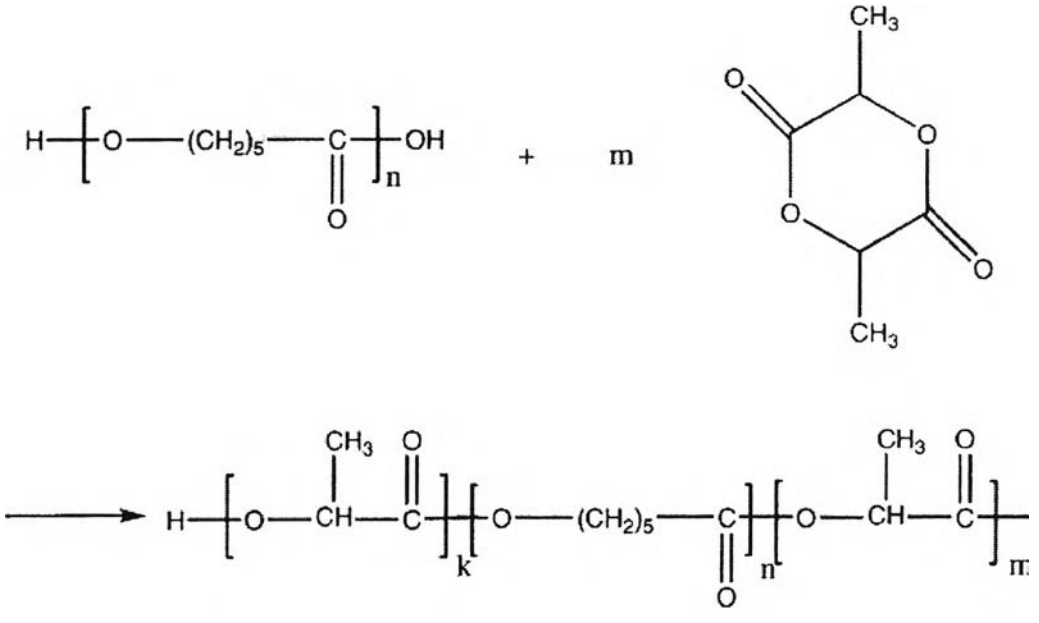

Figure 2.4 Reaction scheme for blockcopolymerisation using pre-oligomerised blocks of one monomer (o-caprolactone) and a second monomer (lactide).

In the next years, Schmack G. et al., (2001) prepared the biodegradable fibres spun from poly(lactide) generated by reactive extrusion. The study was carried out to investigate the PLA in a high speed melt spinning and spin drawing process. The PLA was an amorphous copolymer of L-lactide (92 wt.%) and meso-lactide (8 wt.%) and was generated by reactive extrusion polymerization. This process allowed the polymerization starting from a catalytically initiated ring-opening procedure of lactide, instead of a discontinuous batch-process. It was shown that the PLA polymerized by means of reactive extrusion, can be spun both in a high speed spinning process with a take-up velocity up to 5000 m/min and in a spin drawing process up to a draw ratio of 6. In addition the effect of the melt spinning conditions on the development of structure in the fibres, on the orientation in the crystalline regions and, especially, on the development of a strain-induced crystalline structure in PLA-filaments and the relation with the textile physical properties were investigated. A stress induced crystallization was proved by WAXS in the PLA fibres spun spinning speeds in the range above 3500 m/min and in those spun in a spin drawing process at

draw ratios of 4-6. The stress induced crystalline and its high level of orientation had the dominant influence on the physical break stress and E-modulus. The maximum physical break stress and the E-modulus observed in the spin drawn fibres were about 460 MPa and 6.3 GPa, respectively, with an elongation at break of 24%.

In 2000, Jin H.J. et al., attempted to reduce the brittleness of poly(L-lactic acid) (PLLA) by blending with poly(cis-1,4-isoprene) (PIP). However, the PLLA proved to be incompatible with PIP. PIP was then grafted with polyvinyl acetate (PVAc) to yield PIP-g-PVAc, which was also blended with PLLA because PVAc had been shown to be compatible with PLLA. Compatibility and tensile properties of these blends were investigated. The modulus of PLLA was quite high, but the elongation and toughness were low. The modulus of the PLLA/PIP blend decreased and the elongation and toughness also decreased. However, when PLLA was blended with PIP-g-PVAc, the modulus, elongation, and toughness of PLLA/PIP-g-PVAc blend were improved simultaneously, compared with those of the PLLA/PIP blend. It is interesting to note that the tensile properties of the compatible PLLA/PIP-g-PVAc blend were superior to those of the incompatible PLLA/PIP blend, although the molecular weight of PIP-g-PVAc copolymer was lower than that of PIP. It might be due to the fact that the interfacial bonding with PLLA and PIP-g-PVAc was significantly improved.

Michel A. *et al.*, (2007) focused on the incorporation of dry starch into PLA to reduce the cost of the material while maintaining biodegradability. In this case, the starch acts as filler increasing the rigidity of the material but at the same time further increasing the intrinsic brittleness of the PLA. The starch concentration at which useful materials can be prepared is therefore limited to a low range after which the composite properties suffer dramatically. This has prompted investigations on PLA plasticization as a mean to decrease the brittleness of the composites. This avenue decreases the glass transition of the PLA and can increase the crystallinity level that can be achieved over time in the PLA crystallization temperature range. The use of potential plasticizers such as poly(ethylene glycol), poly(propylene glycol), citrates, glycerol and sorbitol have been investigated in concentrations up to

25%. Acetyl triethyl citrates and triethyl citrate were shown to be the most effective in decreasing the glass-transition of the PLA. At starch concentrations of 40 wt%, the elongation at break of the blends was shown to be very low, below 5% for the materials plasticized with the polyols. For the ones plasticized with 20-25% citrates, elongation at break reached 15% but only at the expense of a 10-fold decrease in tensile modulus and a 4-fold decrease in tensile strength. It is therefore clear that plasticization of the PLA/starch blend offers a relatively limited property range for the resulting composites. This situation was virtually unchanged by using starches with varying amylose content or moisture content.

Li H. *et al.*, (2007) investigated the effect of nucleation and plasticization on the crystalline content of PLA. Combining nucleating agents and plasticizers could have a synergistic effect on PLA crystallization kinetics, due to the improved chain mobility and the enhanced nucleating ability. The nucleating ability of talc, sodium stearate and calcium lactate was assessed while ATC and PEG were used as plasticizers. The crystalline content and properties achieved in different conditions are compared using DSC, tensile mechanical testing and dynamic mechanical analysis. Figure 2.5 presents the effects of PEG or ATC plasticizer content on crystallinity developed for the PLA formulations with 1% talc. At 30 °C mold temperature, the samples were all nearly amorphous. At 80 °C molding temperature, the formulations developed substantial crystallinity. The crystallinity increased from 30 to 40 J/g, as the plasticizer content was increased to 5% and then reached a plateau. There was no obvious difference between the crystallinity developed with PEG or ATC plasticizers.

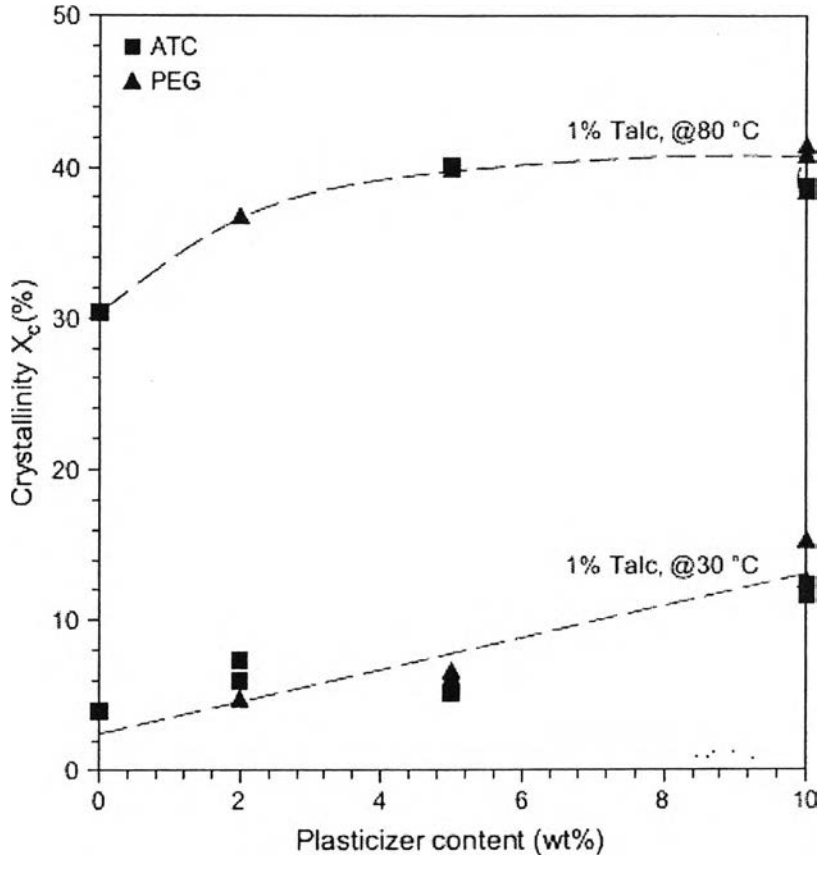

Figure 2.5 Effect of plasticizer content on crystallinity developed at 30 and 80 °C mold temperatures.

Plasticization decreases the glass transition temperature and generally reduces the tensile modulus and tensile strength of amorphous polymers. However, in the case of slowly crystallizing polymers such as PLA, the increase in crystallinity due to enhanced chain mobility can partially or completely offset the plasticization effect. To investigate the interaction between plasticization and crystallization, the neat PLA and the formulations with plasticizers and/or talc were injection molded at 30 and 80 °C to generate nearly amorphous and fully crystallized sample, respectively. Table 2.3 presents the tensile modulus, strength and elongation along with the achieved crystallinity. The amorphous PLA presented high tensile modulus and tensile strength at 3.7 GPa and 70 MPa, respectively, and a relatively low elongation at break, around 5%. It was not possible to prepare fully crystallized neat PLA but formulation comprising as little as 1% talc could be fully crystallized when using a high

mold temperature. Surprisingly, the tensile properties of these crystallized samples are similar to those of the amorphous neat PLA. It has been postulated that this absence of effect is due to the weak linkage between the amorphous and crystalline phases of PLA. A second observation concerns the effect of the plasticizer. In absence of talc, the molded samples were nearly amorphous regardless of the plasticizer contents or molding temperature. For 2-5% ATC plasticizer concentration, the modulus was nearly unchanged and dropped only to 3.2-3.3 GPa when 10% ATC was added. Tensile strength dropped more steadily with plasticizer content with values dropping to 50-53 MPa at the 10% ATC level. The elongation was nearly unaffected at these plasticizer levels and remained below 10%. The sole effect of PEG (in absence of talc) was not investigated but it could be expected to follow similar trends. The next important observation concerns the effect of simultaneous addition of plasticizer and of the talc, nucleating agent. In this case, the mold temperature significantly affected the crystallinity. All these formulations had a low crystallinity, below 15% when injected in a mold held at 30 °C. In this case the properties were similar to those of the plasticized formulations without talc as expected from their similar crystallinity levels. When mold temperatures of 80 °C were used, the samples were all close to being fully crystallized and in this case a peculiar phenomenon was observed. The tensile data for 2 and 5% plasticizer were similar to those reported for the more amorphous samples of similar plasticizer level, but suddenly at the 10% plasticizer level the modulus and tensile strength dropped almost by a factor of 2. Conversely, the elongation at break increased dramatically to 40 and 70% for 10% PEG and ATC, respectively. Since the plasticizer cannot be included within the crystals, a possible cause for this dramatic change can be the expulsion of the plasticizer from the crystallizing regions which in turn will increase the local plasticizer concentration in the amorphous regions. Prior work in ATC and PEG-plasticized amorphous PLA formulations showed that a dramatic ductility increases occurred only when at least 15% ATC or 20% PEG were used. In our case, the expulsion of the plasticizer out of the crystallizing regions that accounts for around 40% of the volume, can push the local plasticizer concentration in the amorphous regions in this critical concentration range.

Table 2.3 Tensile modulus, strength and elongation at break and crystallinity as a function of formulation and molding temperature

Plasticizer (wt%)	Talc (wt%)	Mold temperature (°C)	%X	Tensile properties, average (STD)		
				E (GPa)	σ (MPa)	ε_b (%)
0	0	30	6	3.68 (±0.13)	69.2 (±0.41)	6.0 (±0.29)
		80	14	3.70 (±0.10)	70.2 (±1.09)	5.8 (±0.32)
0	1	30	4	3.79 (±0.12)	63.9 (±0.77)	7.5 (±0.63)
		80	30	4.03 (±0.39)	67.7 (±0.71)	4.7 (±0.61)
2% ATC	0	30	<5	3.49 (±0.07)	64.3 (±0.68)	8.8 (±1.78)
		80	<5	3.54 (±0.24)	68.0 (±0.61)	6.0 (±0.31)
5% ATC	0	30	7	3.46 (±0.05)	57.8 (±1.32)	5.2 (±0.34)
		80	12	3.62 (±0.16)	59.2 (±1.94)	4.6 (±0.56)
10% ATC	0	30	<5	3.15 (±0.08)	50.1 (±0.28)	6.1 (±1.30)
		80	<5	3.32 (±0.17)	52.6 (±0.59)	4.6 (±0.07)
2% ATC	1	30	7	3.65 (±0.04)	60.1 (±0.18)	10.6 (±2.42)
		80	22	3.80 (±0.39)	65.4 (±0.84)	6.8 (±0.45)
5% ATC	1	30	5	3.59 (±0.07)	55.4 (±0.59)	9.0 (±3.34)
		80	36	3.75 (±0.21)	60.9 (±0.89)	5.3 (±1.39)
10% ATC	1	30	12	3.22 (±0.09)	47.3 (±0.98)	6.5 (±4.94)
		80	39	2.16 (±0.11)	34.5 (±0.37)	73.9 (±24.0)
2% PEG	1	30	5	3.70 (±0.14)	60.5 (±0.76)	10.5 (±4.61)
		80	37	4.23 (±0.02)	67.8 (±0.77)	6.2 (±1.88)
5% PEG	1	30	6	3.56 (±0.10)	54.5 (±0.96)	9.1 (±7.02)
		80	40	3.61 (±0.07)	53.8 (±0.28)	9.5 (±6.29)
10% PEG	1	30	14	3.02 (±0.07)	44.8 (±0.97)	39.9 (±37.2)
		80	41	2.39 (±0.05)	37.3 (±0.19)	40.4 (±14.6)

In 2007, Bhardwaj R. *et al.*, reported the creation of a novel polylactide (PLA)-based nanoblend by in-situ generation of new hyperbranched polymer (HBP)-based nanostructures in the matrix polymer prepared via an environmentally friendly melt processing technique. Figure 2.6 schematically depicts the in-situ cross-linking of HBP with PA in the PLA matrix performed during melt processing of PLA.

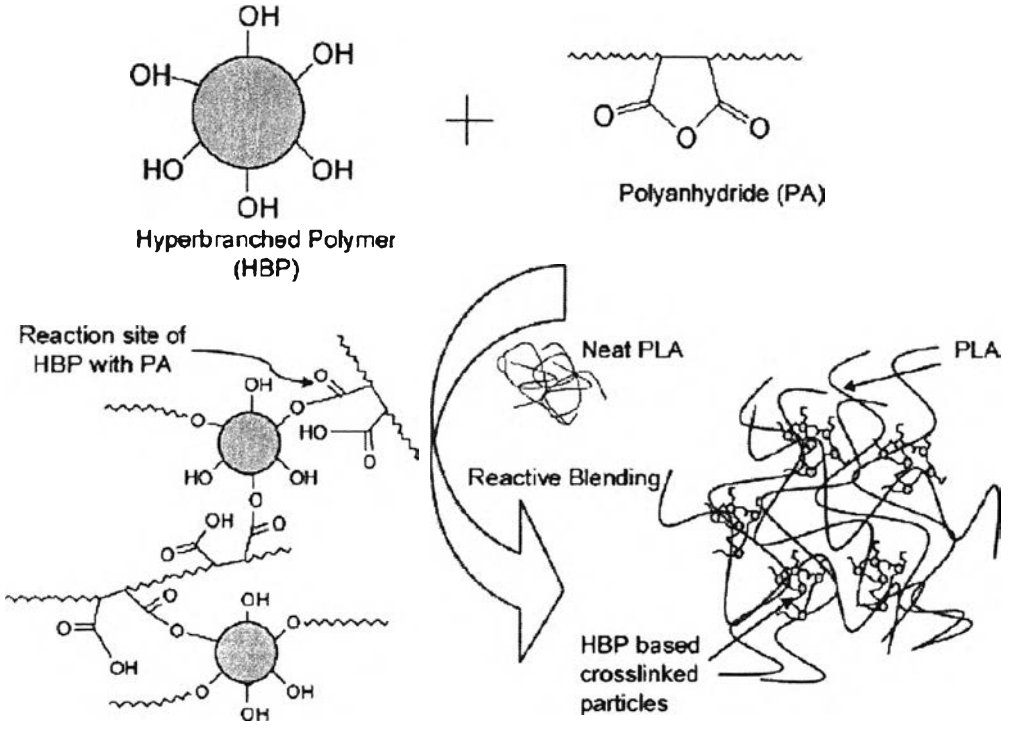

Figure 2.6 Schematic illustrations of in-situ cross-linking of hyperbranched polymer (HBP) in the PLA melt with the help of a polyanhydride (PA).

Low temperature dynamical mechanical thermal analysis (DMTA) was conducted to observe the cross-linking of HBP, phase separation, and molecular interaction of PLA with HBP and cross-linked HBP (cHBP). The temperature dependency of loss modulus (E'') of neat PLA, PLA/HBP (92/08) blend, and PLA/HBP/PA (92/5.4/2.6) blend is shown in Figure 2.7. In the PLA/HBP (92/08) blend, there were two loss modulus (E'') relaxation peaks at -40 °C and 58 °C, respectively, corresponding to the glass transition temperature (T_g) of HBP and PLA, respectively. There was slight depression in the T_g of PLA in the presence of HBP. It suggested that there was some molecular interaction between PLA and HBP, but this system was dominated by phase separation. Phase separation has also been a major problem in most of the plasticized PLA systems. The creation of free volume in plasticized PLA enhances its molecular mobility, facilitating the increase in its crystallinity, which renders the expulsion of plasticizer molecules from the amorphous region.

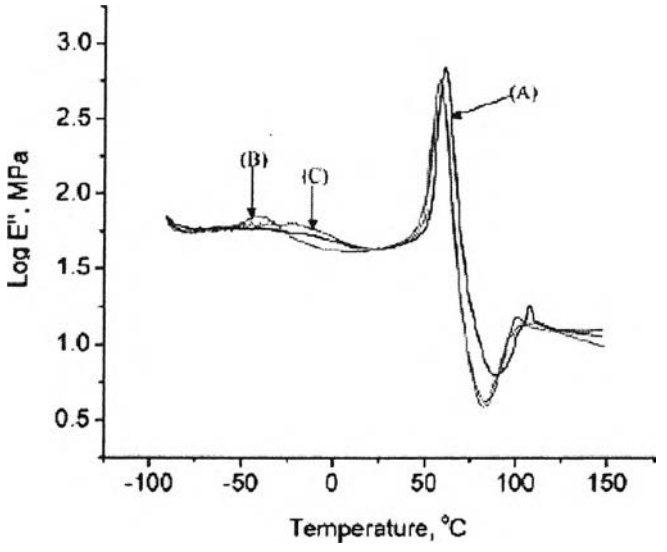

Figure 2.7 Temperature dependence of the loss modulus (E¢¢) of (A) neat PLA, (B) PLA/HBP (92/08) blend, and (C) PLA/HBP/PA (92/5.4/2.6) blend. The shift in the glass transition temperature (T_g) of HBP from -40 °C to -31 °C indicated the occurrence of cross-linking of the HBP.

Stress-strain curves of neat PLA, PLA/HBP (92/08), and PLA/HBP/PA (92/5.4/2.6) blends are shown in Figure 2.8. There was no improvement of elongation at break value of PLA when blended with 8 wt.% of pristine HBP as well as with 2.7 wt.% of PA, but the elongation at break of PLA was improved by around 847% for the PLA/HBP/PA (92/5.4/2.6) blend. The PLA and PLA/HBP (92/08) blends underwent strain softening and deformed in brittle fashion. On the other hand, the PLA/HBP/PA (92/5.4/2.6) blend showed initial strain softening after yielding and then underwent considerable cold drawing. The stress-strain curve after the yield point showed a combination of strain softening and cold drawing. In this region, there was competition between PLA chain orientation and crack formation. Hence, there was a drop in stress with increasing strain. After 20% of strain, only cold drawing dominated at a constant stress. This suggested that a large energy dissipation occurred in the presence of cross-linked HBP particles in the PLA/HBP/PA (92/5.4/2.6) blend. The toughness, calculated as the area under stress-strain, exhibited a drop in its value for the PLA/HBP (92/08) blend as compared to the neat PLA,

while increased dramatically from 2.6 MJ/m^3 for neat PLA to 17.4 MJ/m^3 for the PLA/HBP/PA (92/5.4/2.6) blend. This was quite an unusual result, as the modified PLA maintained a quite high tensile modulus value of 2.8 GPa. The result was very significant in obtaining a biobased material having remarkable stiffness-toughness balance. The tensile strength of modified PLA decreased to 63.9 MPa from 76.5 MPa for neat PLA. These results suggested that the nanoscale cross-linked HBP particles behaved like rubber particles and were effective in improving the toughness of PLA at low concentration (8 wt.%) with a minimal sacrifice of tensile strength and modulus.

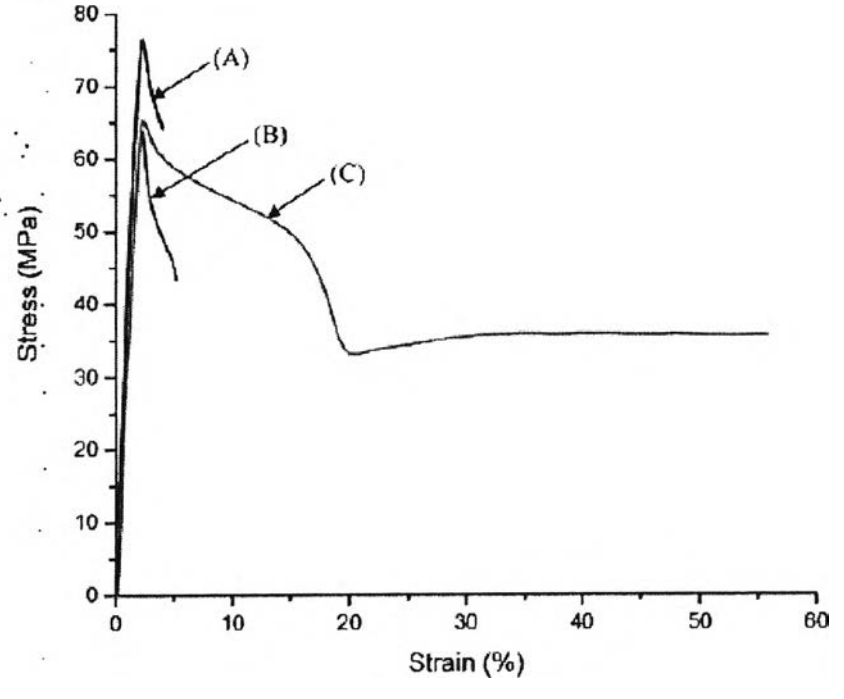

Figure 2.8 Stress-strain curves obtained at a cross-head speed of 15.4 mm/min: (A) neat PLA; (B) PLA/HBP (92/08); (C) PLA/HBP/PA (92/5.4/2.6).

Figure 2.9 represents the scanning electron micrographs of the tensile fractured surfaces of neat PLA, PLA/HBP (92/08) blend, and PLA/HBP/PA (92/5.4/2.6) blend. The surface of neat PLA was extremely flat, indicating the brittle failure of PLA under tensile loading. The tensile fractured surface of PLA/HBP (92/08) revealed inhomogeniety, formation of voids, and absence of ductile tearing. This was

an indication of phase separation, incompatibility between the PLA and HBP, and brittle failure. The in-situ cross-linking of HBP in the PLA matrix dramatically changed its surface characteristic after deformation. The tensile fractured surface of the PLA/HBP/PA (92/5.4/2.6) blend exhibited considerable ductile tearing, surface roughness, and surface integrity. The increased surface area of fractured surface of the PLA/HBP/PA (92/5.4/2.6) blend suggested that the crack paths were highly bifurcated, and crack propagation absorbed considerable strain energy before failure. This led to a conclusion that the in-situ cross-linking of HBP was instrumental in improving the compatibility between the PLA and HBP phase and resulted in significant toughness enhancement of PLA bioplastic.

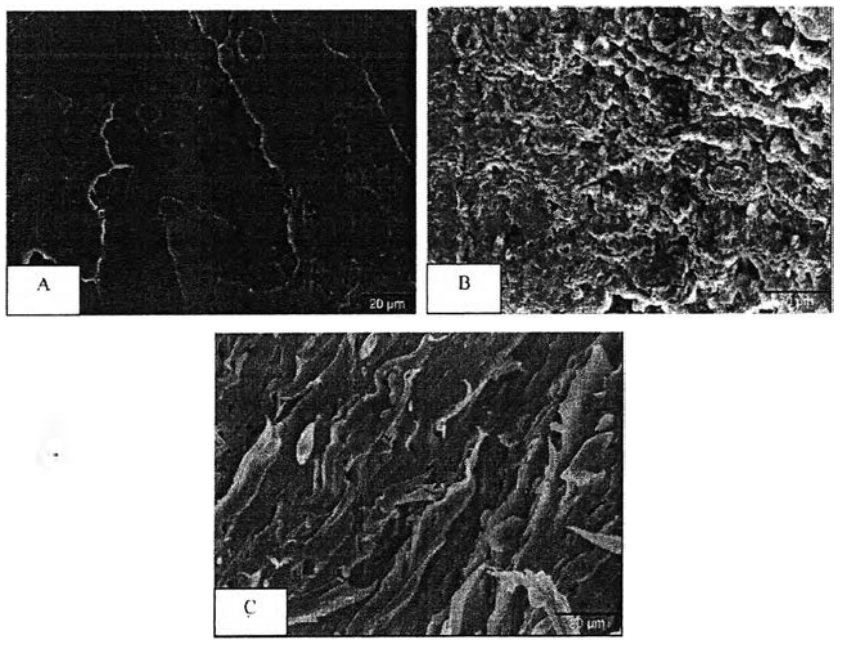

Figure 2.9 Scanning electron micrographs of tensile fracture surfaces: A: Neat PLA; B: PLA/HBP (92/08); C: PLA/HBP/PA (92/5.4/2.6).

Raquez J. *et al.*, (2006) reviewed about various strategic pathways to produce biodegradable polyesters and related compatibilized melt blends by reactive extrusion (all steps conducted in a twin-screw extruder): polyester synthesis by continuous catalyzed ring-opening polymerization when Tin and aluminium-based catalysts would be considered for quantitatively converting the cyclic monomer in high

molecular weight polyester chains within residence time of a few minute only, polyester chemical modification (self-branching) and chain-functionalization (maleation), and compatibilization of poyester melt blends with different naturally occurring fillers. PLAs produced in single-stage contiuous REX polymerization were compared to PLAs produced in glass ampouled using bulk batch polymerization technology on the basis of molecular parameters (Table 2.4). The resulting conversion showed that both of polymerization reactions had been finished. PLA chains had been chemically modified by grafting reaction of maleic anhydride (MA) (maleation reaction) induced by a free-radical process performed in bulk through REX. MA-grafted PLA (MAG-PLA) with 0.65 wt.% MA had been melt blended with granular corn starch in an internal mixer. PLA/starch interfacial interactions were improved by using MA-grafted polyester chains. This resulted from the strong interactions between carboxylic anhydrides and the hydroxyl functions of the polysaccharide chains.

Table 2.4 Comparion between PLAs as produced in bulk either in traditional batch processing or in REX polymerization in a co-rotating closely intermeshing twin-screw extruder, both promoted by an equimolar $Sn(Oct)_2{\cdot}P(C_6H_5)_3$ complex with a $[L\text{-}LA]_0/[Sn]$ ratio of 5000, at 180 °C (extrusion throughput ~1 kg/h) M_w/M_n Polymer conversion %. Maleation reaction or REX-PLA via a free-radical process

Entry	Process	Time for Conversion (min)	conversion %	M_n	M_w/M_n
1	Batch	40	98.5	246000	1.9
2	REX	~7	99	91100	1.8

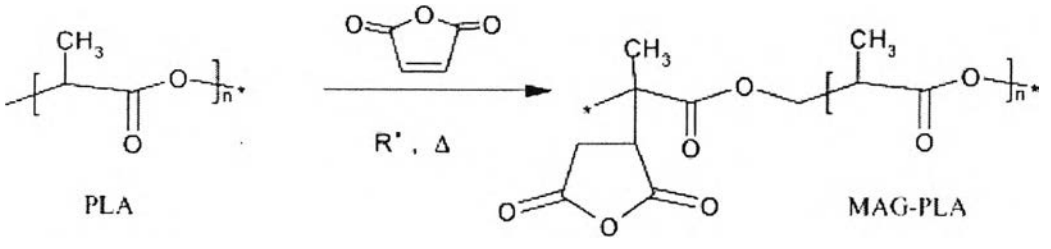

Figure 2.10 The grafting reaction of maleic anhydride (MA) onto the PLA backbone had been performed through a free-radical process again conducted by REX.

Janata M. *et al.*, (2003) sythesized the polystyrene and polystyrene-block-poly(methyl methacrylate) densely grafted with poly(ε-caprolactone) or poly(DL-lactide) in the benzene rings by "geafting from" method. Polystyrene and polystyrene-block-poly(methyl methacrylate), both ring-substituted with 1-hydroxyethyl group, as procursurs for the grafting. Ring-opening polymerization of ε-caprolactone or DL-lactide initiated with the hydroxyl group and co-initiated/catalyzed with stannous octoate. Successful grafting of ε-caprolactone or DL-lactide from this hydroxylated PS (Scheme 1) and from the hydroxylated PS-b-PMMA copolymer (Scheme 2) were confirmed by SEC and NMR spectra. SEC traces of both isolated graft copolymers (polystyrene-graft-poly(ε-caprolactone), polystyrene-graft-poly(DL-lactide), [polystyrene-graft-poly(ε-caprolactone)]-brock-poly(methyl methacrylate), and [polystyrene-graft-poly(DL-lactide)]-block-poly(methyl methacrylate)) were unimodal and no peak of corresponding homopoymers (polycaprolactone and polylactide), often formed as by-products in grafting, were observed. SEC analysis showed an increase in molecular weight of graft copolymers as compared with that of the starting hydroxylated PS and PS-b-PMMA. The MWDs of the graft copolymers were narrow. ^{1}H NMR spectra of graft copolymers demonstrated 100% grafting efficiency. In other words, all free hydroxyl groups of the hydroxylated PS effectively initiated the ROP of ε-caprolactone or DL-lactide.

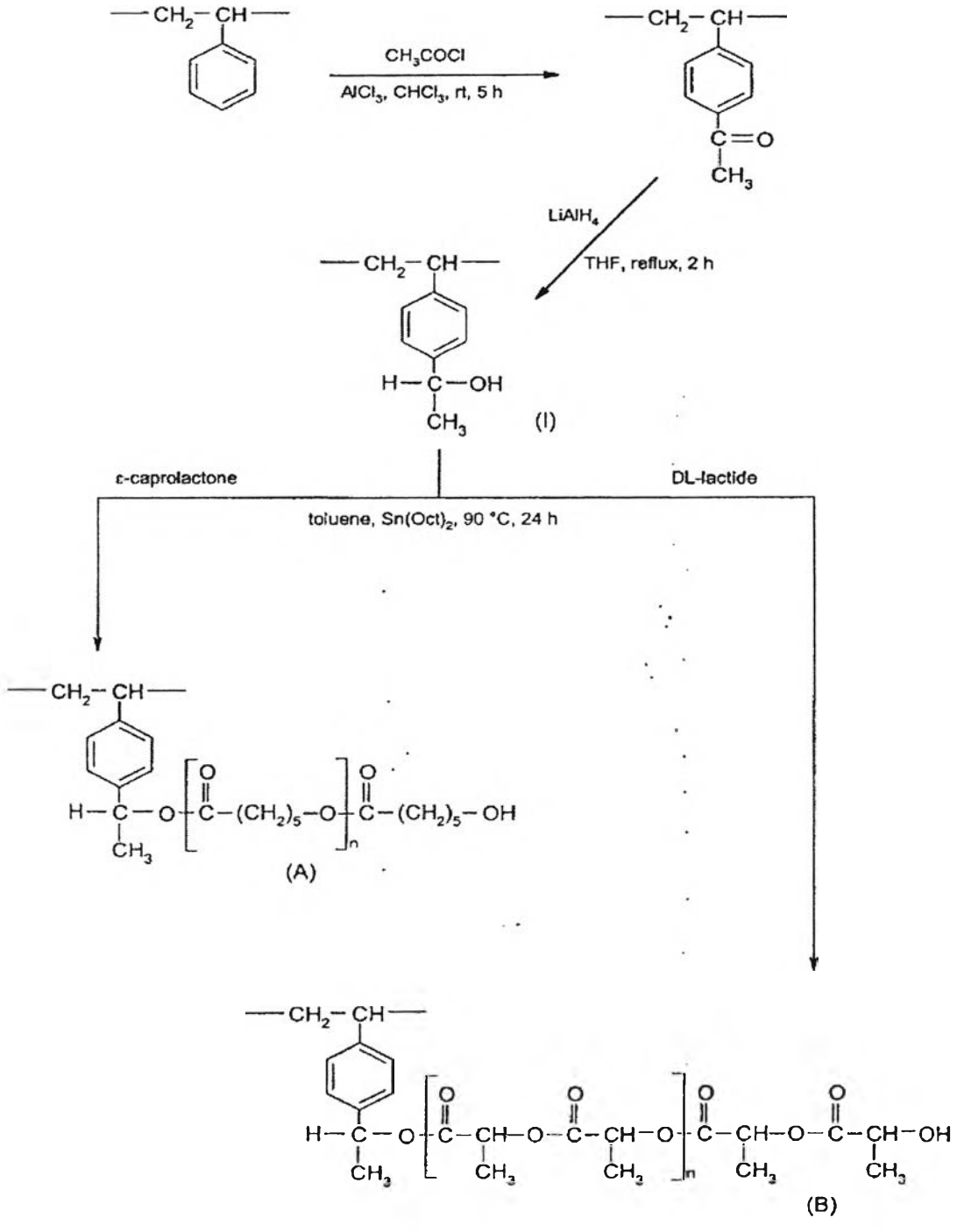

Scheme 1.

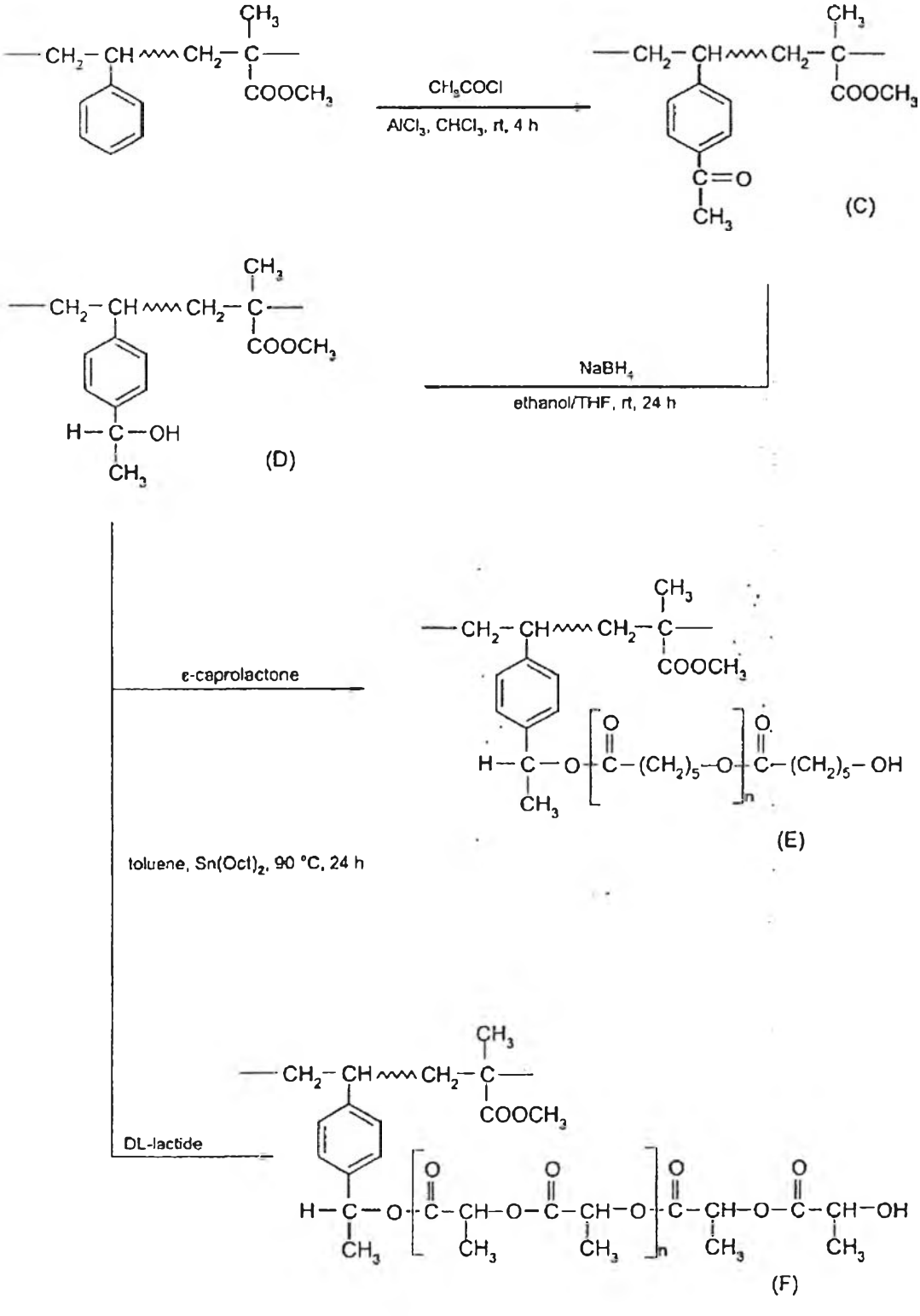
CH3COCl
AlCl3, CHCl3, rt, 4 h
(C)
NaBH4
ethanol/THF, rt, 24 h
(D)
ε-caprolactone
toluene, Sn(Oct)2, 90 °C, 24 h
(E)
DL-lactide
(F)

Scheme 2.

In 2003, Rosales C. *et al.*, studied the grafting of two commercial polyethylenes, low-density polyethylene and linear low-density polyethylene with diethyl maleate carried out in a corotating twin-screw extruder at different extrusion conditions. The effects of the grafting degree and the processing conditions used in the preparation of the functionalized materials on their shear and elongational viscosities at high shear rates, and on their thermal and tensile properties were also studied. The increase in screw speed should result in a decrease of residence time and, therefore, in the degree of grafting (Figure 2.11). However, it also resulted in an increase of the mixing in the extruder, thereby increasing the degree of grafting. For thermal properties, the grafting degree increased, the crystallinity content of the materials seemed to decrease. The introduction of maleated units in the chain conferred more imperfections to the microstructural regularity of the polymer crystal, leading to a reduction of the mean lamellar thickness of the grafted materials: The tensile properties, a decrease in the elastic modulus in the sample with the highest grafting degree could be observed. That decrease could be attributed to a decrease in its crystallinity content.

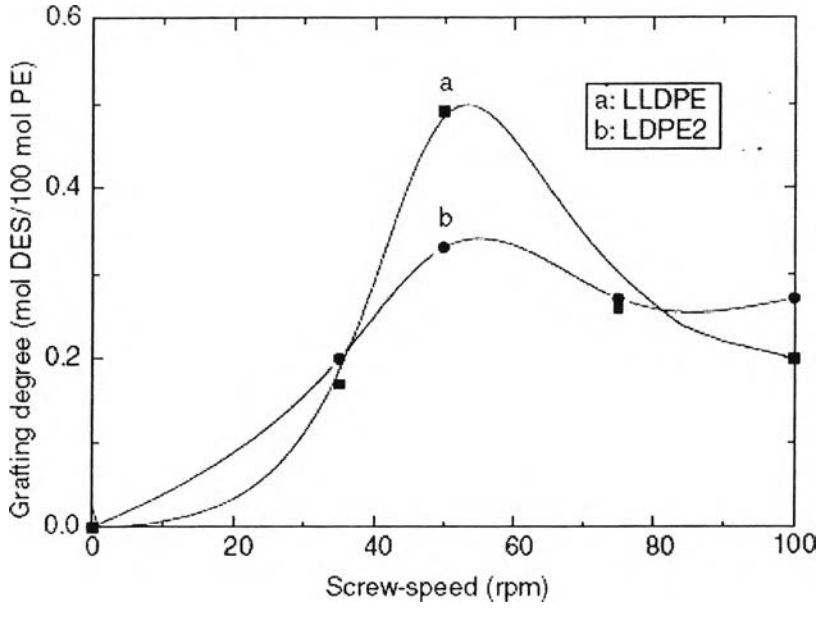

Figure 2.11 Grafting degree as a function of the screw-speed for LDPE-g-DEM materials.

Cai Q. et al. (2003) synthesized brush-like biodegradable polylactide-grafted dextran copolymer (PLA-g-dextran) by a bulk polymerization reaction using a trimethylsilyl-protected (TMS) dextran as macroinitiator and stannous octoate as catalyst. The PLA-g-dextran copolymers were characterized by 1H NMR, GPC and intrinsic viscosity measurements. The synthesis of the PLA-g-dextran was confirmed by ^{1}H NMR determination (Figure 2.12, lower). Using $CDCl_3$ without tetramethylsilane as solvent, the ^{1}H NMR spectra of the polylactide products initiated by TMSD exhibited clear signals around 0.1–0.5 ppm, which were attributed to the trimethylsilyl groups. Besides, several weak broad peaks were found around 3.5–5.5 ppm belonging to the -CH or -CH_2 of glucose units. After the products were suspending in methanol at room temperature for two days to remove the TMS groups, the methyl proton signals of TMS groups below 0.5 ppm disappeared, but the weak broad signals around 3.5–5.5 ppm still existed (Figure 11, upper). The methylene and methylidyne signals of dextran were so broad and extremely weak, because the content of glucose units was low and the mobility of the sugar units was very low in $CDCl_3$. It was interested to point out that the inherent viscosity of PLA-g-dextran copolymer increased a little after de-protection, e.g. it could increase to 1.86 dl/g from original 1.68 dl/g, which was considered due to the weak hydrogen bond between hydroxyl groups existing on the dextran backbone.

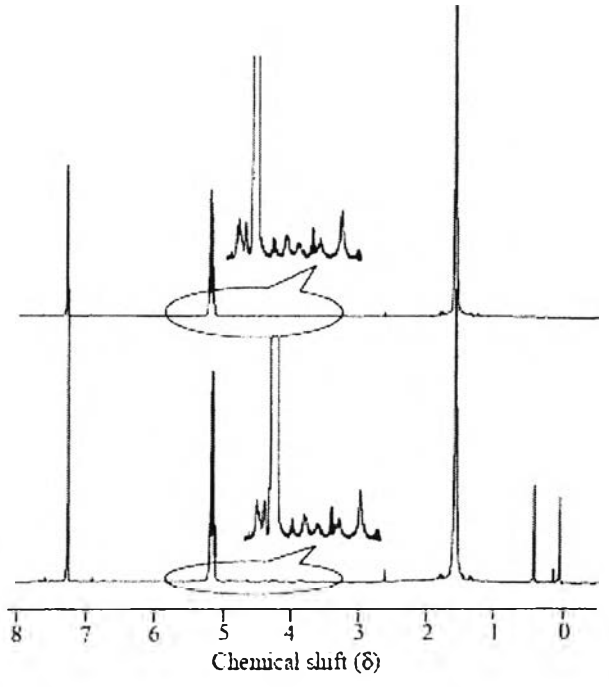

Figure 2.12 ^{1}H NMR spectra of PLA-g-dextran before (lower) and after (upper) de-protection of trimethylsilyl groups in methanol.

In 2006, Yin J., studied poly(ethylene-vinyl acetate) (EVA) copolymer melt grafted with maleic anhydride (MAH) in a twin screw extruder in the presence of peroxide. It is confirmed that MAH has been melt grafted on the backbone of EVA by FTIR. Infrared spectra corresponding to pure EVA and functionalized EVA are shown in Figure 2.13. Unfortunately, the presence of peaks at 1790 and 1865 cm^{-1}, characteristic of the carbonyl in the MAH, cannot be observed clearly because of the existence of acetoxy carbonyl carbon of the VA unit, which covers other bands in this zone. Only a few peaks in 1790 and 1865 cm^{-1} are checked in the spectra of grafted EVA with comparison to that of pure polymer, which might confirm the grafting reaction between EVA and MAH. To weaken the influence of VA group on FTIR analysis, the method of hydrolysis is performed, which is also believed to be useful for determining the mechanism of grafting reaction in EVA. The hydrolysis products of EVA and EVA-*g*-MAH are expressed as EVAL and EVAL-*g*-MAH, respectively. The FTIR spectra are shown in Figure 2.14. Comparison with the spectra of EVA and EVA-*g*-MAH, the characteristic peak of carbonyl on VA group is

sharpen and weaken but still exists, which is attributed to the strong absorption of carbonyl and also an indication of incomplete hydrolysis process in our experimental conditions. However, the existence of characteristic band near 1790 cm^{-1} corresponding to the carboxylic groups of MAH is confirmed, which should be regarded as the evidence of grafting reaction, since no similar band appears in the spectra of EVAL. It is worthy noticing here that the FTIR analysis on hydrolysis product of EVA and its grafting samples prove the grafting reaction of MAH on the hydrogen atom of tertiary carbon at EVA main chain, otherwise, the peaks of MAH should disappear if the reaction takes place entirely in the hydrogen atoms of methyl units on VA groups.

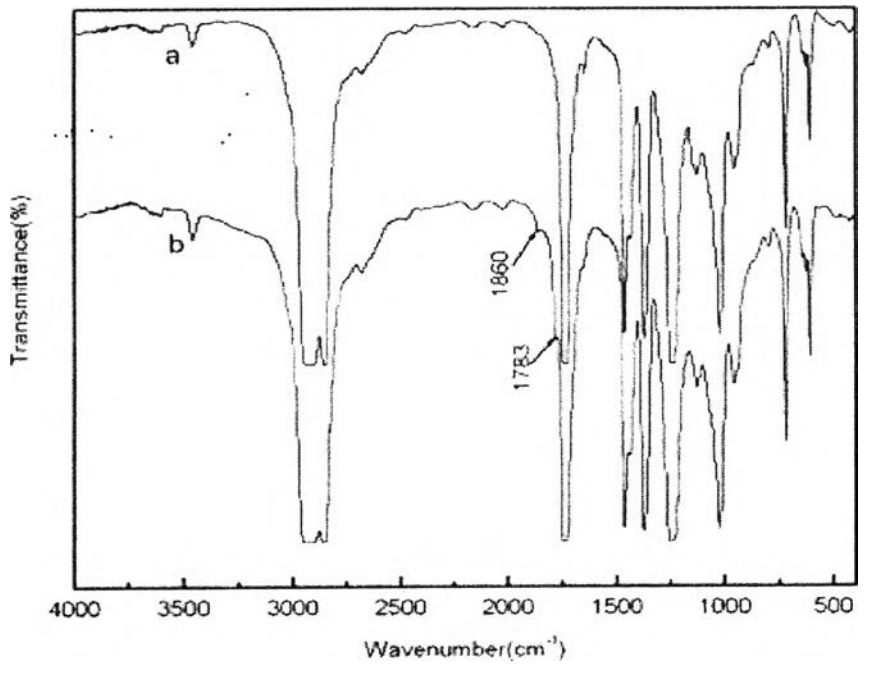

Figure 2.13 FTIR spectra of (a) EVA and (b) EVA-g-MAH.

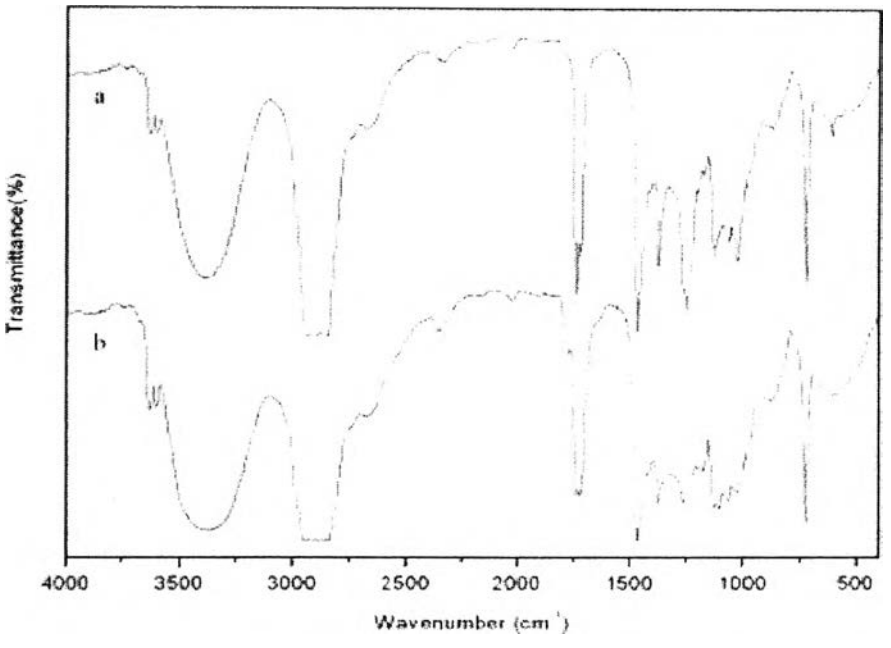

Figure 2.14 FTIR spectra of (a) EVAL and (b) EVAL-g-MAH.

Liu Y. (2004) synthesized and characterized a brush-like copolymer of polylaluminum as catalyst in toluene at 70 °C. It was found that a greater lactide content in the feeding ratio results in a higher grafting percentage. The grafting percentage and the amount of lactide introduced to chitosan increase with feeding molar ratio are shown in Table 2.5. When the feeding molar ratio of lactide to chitosan increased from 2:1 to 40:1, the grafting percentage rose from 43% to 462%; meanwhile, the molar of lactide to chitosan in the copolymer also rose from 0.96 to 10.33. This indicates that the higher the concentration of lactide in the toluene, the higher opportunity for the lactide to react with chitosan reactive centers.

Table 2.5 The lactide grafted onto chitosan copolymer in toluene at 70 °C with Et_3Al as catalyst

Molar ratio (lactide:chitosan)	Total yield (%)	Grafting percentage (%)
2:1	50.4	43
5:1	38.1	109
6:1	32.8	136
10:1	43.8	338
20:1	26.7	408
40:1	15.2	462

Figure 2.15 shows the WAXS patterns as compared with that of chitosan. The strongest reflection of chitosan appears at $2\theta = 19.84°$. In the feeding ratio, the ratio of lactide to chitosan is 2:1, the strongest reflection shifts to $2\theta = 19.74°$. In the case of 5:1 and 6:1, it is $2\theta = 21.66°$ and 21.44°, respectively. These results indicate the crystalline patterns were different with chitosan, when lactide was grafted onto it; the original crystallinity was destroyed. The strongest peak appears at about $2\theta = 16.7°$ for samples of 10:1, 20:1, 40:1, which changes more remarkably than the ones mentioned above. In addition to that, these three samples have almost the same d-spacing, which means that graft copolymers have a similar packing mode when the graft percentage is >338% (in the feeding ratio 10:1).

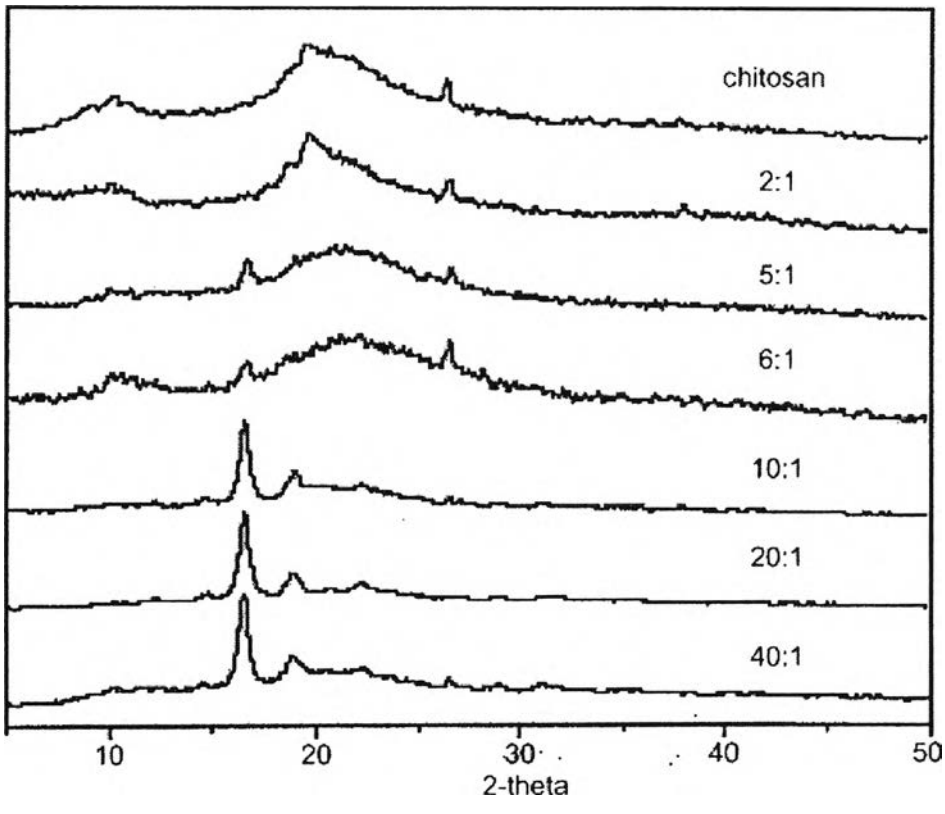

Figure 2.15 WAXS patterns of chitosan and its graft copolymer: (a) chitosan, (b) 2:1, (c) 5:1, (d) 10:1, (e) 20:1, (f) 40:1.

Lee C. M. (2005) studied reactive blending of poly(lactic acid) with poly(ethylene-co-vinyl alcohol) in the presence of an esterification catalyst to induce reaction between the hydroxyl groups of EVOH and the terminal carboxylic group of PLLA. EVOH was selected for the host polymer, because it has hydroxyl groups to be reacted with PLLA and also has excellent processability as well as good mechanical properties. Tetrabutyl titanate was used as a catalyst to induce reaction between EVOH and PLLA. Tensile properties of the resulting graft copolymer (EVOH-*g*-PLLA) are shown in Table 2.6. When the low-molecular-weight PLLA was reacted with EVOH, the resulting EVOH-*g*-PLLA retained good tensile properties up to a content of PLLA as high as 60 wt %; and, thereafter, elongation at break of the EVOH-*g*-PLLA decreased sharply. It is worth noting that elongation at break of EVOH-*g*-PLLA containing 40 wt % of PLLA (EVOH-*g*-PLLA 40) was eight times higher than that of an EVOH/PLLA 60/40 simple blend.

Table 2.6 Tensile properties of PLLA/EVOH blends

Blend composition (%)	E. modulus (MPa)	Max stress (MPa)	Elong at break (%)
PLLA	—	—	—
EVOH-*g*-PLLA 80	1303 ± 493.3	0.55 ± 0.35	1.77 ± 0.55
EVOH-*g*-PLLA 60	1711 ± 385.0	1.78 ± 0.58	9.34 ± 18.9
EVOH-*g*-PLLA 50	1661 ± 412.9	1.59 ± 0.72	12.2 ± 8.12
EVOH-*g*-PLLA 40	1198 ± 392.3	1.16 ± 0.15	21.6 ± 5.51
EVOH-*g*-PLLA 20	1447 ± 355.9	1.43 ± 0.65	9.44 ± 2.97
EVOH	1067 ± 453.2	1.98 ± 0.62	16.5 ± 4.62
EVOH/PLLA 60/40	860 ± 643.1	1.73 ± 0.77	2.70 ± 1.28

Figure 2.16 shows the second scan DSC thermogram of PLLA, EVOH, EVOH-*g*-PLLA, and EVOH/PLLA 60/40 blend. The EVOH/PLLA 60/40 blend shows two separate melting peaks located at around the melting temperatures of the corresponding parent polymers, indicating that the two polymers are phase-separated. Crystallization peak temperature (T*c*) was determined by cooling from 200 °C at -20 °C/min. T*m* and Δ*Hf* were observed while reheating the cooled sample from 30 °C at 20 °C/min. The EVOH/PLLA 60/40 blend had almost the same T*c* at 94 °C as that of EVOH. In contrast, T*c* of EVOH-*g*-PLLA 40 appeared at 88 °C, which was 6-8 °C lower than that of EVOH/PLLA 60/40. Therefore, it can be said that PLLA grafted to EVOH significantly suppressed the crystallization of the EVOH moiety. T*m* of the EVOH phase in EVOH-*g*-PLLA shifted to a lower temperature region as the content of PLLA increased. The T*m* peak of the PLLA phase did not show up until the content of PLLA was higher than 60 wt %.

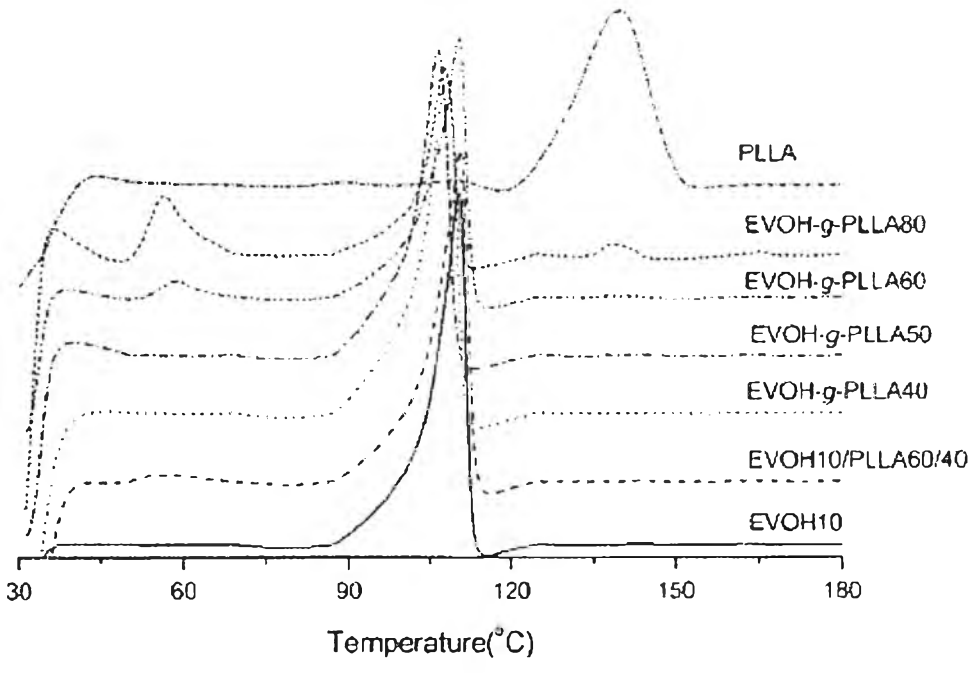

Figure 2.16 The second scan DSC thermograms of EVOH-*g*-PLLA and EVOH/PLLA blend.